

Reverse Water Gas Shift Reaction

Subjects: Engineering, Chemical | Chemistry, Applied | Nanoscience & Nanotechnology

Contributor: Parisa Ebrahimi, Anand Kumar, Majeda Khraisheh

The catalytic conversion of CO₂ to CO by the reverse water gas shift (RWGS) reaction followed by well-established synthesis gas conversion technologies could be a practical technique to convert CO₂ to valuable chemicals and fuels in industrial settings. For catalyst developers, prevention of side reactions like methanation, low-temperature activity, and selectivity enhancements for the RWGS reaction are crucial concerns. Cerium oxide (ceria, CeO₂) has received considerable attention due to its exceptional physical and chemical properties.

Keywords: reverse water gas shift reaction ; mechanism and kinetics ; CeO₂ support

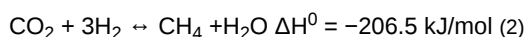
1. Introduction

Carbon dioxide has been identified as the primary anthropogenic greenhouse gas that has resulted in catastrophic climate change and ocean acidification ^{[1][2]}. Various approaches have been employed to reduce the amount of CO₂ in the atmosphere. For example, power-to-liquid (PtL) sustainable aviation fuel (SAF) was recently proposed as a long-term and scalable solution to minimize aircraft CO₂ emissions. The procedure turns CO₂ into a synthetic fuel with less sulfur and fewer aromatics, which enhances local air quality and minimizes the effect of aviation at high altitudes ^[3]. On the other hand, since enormous amounts of low-cost, relatively pure carbon dioxide are available from carbon sequestration and storage facilities, more efforts have been made to utilize CO₂ as an alternative C1 source rather than merely considering it as waste ^[4]. A unique and appealing alternative to storing CO₂ through sequestration would be recycling the gas into energy-rich compounds via carbon capture, storage and utilization (CCSU) ^{[5][6]}. E-fuels, also known as electrofuels or powerfuels, are hydrocarbon fuels produced from hydrogen and CO₂ in which hydrogen is generated from water and electricity through electrolysis and CO₂ is either captured from fossil sources (such as industrial sectors) or the atmosphere ^{[7][8][9]}. E-fuels aim to directly electrify a system without the demand-side adjustments necessary for a direct electrification by substituting fossil fuels with renewable power ^[7]. However, the CO₂ molecule is a relatively inert and unreactive molecule with a high level of thermodynamic and chemical stability due to its linear chemical structure with double bonds connecting the carbon and oxygen atoms, so converting it to the more reactive CO is energy-intensive ^[10]. Among the systems currently available for CO₂ conversion, catalytic conversion to CO, commonly known as the reverse water-gas shift (RWGS) reaction (Equation (1)), is one of the most promising reversible hydrogenation methods that offer a high potential efficiency ^[11].



RWGS reaction is recognized as an important intermediate stage in a number of key CO₂ hydrogenation reactions such as the Sabatier process ^[12] and methanol synthesis ^[13], and is hence referred to as the “building block stage” ^[14]. Synthesis gas (CO + H₂), a crucial precursor in the field of C1 chemistry, can be produced using the RWGS reaction in the presence of an appropriate catalyst. The syngas can further be used as a feedstock for the Fischer–Tropsch synthesis reaction (FTS) to produce organic compounds, such as methanol (a crucial component of synthetic fuels and polymers), hydrocarbons, or oxygenated hydrocarbons ^{[15][16]}. ExxonMobil recently revealed that its “methanol-to-jet” technology can provide SAF from methanol derived through waste, biomass, captured carbon dioxide, and low-carbon hydrogen ^[17]. However, further side reactions, such as CO methanation (Equation (2)) ^[18], could emerge under the same reaction conditions, consuming a large amount of hydrogen. The CO₂ methanation reaction is an exothermic catalytic process that normally takes place at temperatures from 150 °C to 550 °C in the presence of a catalyst ^[19]. The CO₂ conversion and CH₄ selectivity can almost approach 100%; however, as the temperature rises, the reaction rate increases ^[20], with preference for RWGS at higher temperature. Therefore, at low reaction temperatures, the highly exothermic methanation reaction is thermodynamically more preferred to the slightly endothermic RWGS reaction ^{[21][22]}; hence, reducing methanation throughout RWGS has been a challenging issue. A remaining concern seems to be either the RWGS reaction should be operated at high temperature (over 900 °C), which is thermodynamically favorable, but carbon and undesirable byproducts may also be present; or it should be performed at low temperatures (below 500 °C), in which case

it is not kinetically favored but may be made up for by extensive catalyst use [23]. Over the temperature range of 100 to 1000 °C, Kaiser et al. investigated the equilibrium composition of the gaseous products in RWGS reaction for a three-to-one molar H₂/CO₂ input ratio [24]. Based on the results, methanation was thermodynamically preferred at low temperatures (below 600 °C), while, the only product that could form at temperatures beyond 700 °C was CO and very little to no methane. However, to cut down on the energy losses and investment expenses, the temperature must be kept as low as feasible [24]. They proposed that using RWGS at greater pressures in conjunction with high temperature and high-pressure steam electrolysis might be an alternative [24]. Additionally, the FTS normally operates at 2.5 MPa, and the produced syngas or the RWGS supply gas must be compressed [25]. Kaiser et al. came to the conclusion that at this pressure (2.5 MPa), the methane curve was pushed to higher temperatures; for instance, at 900 °C, the equilibrium methane level was 4 mol% as opposed to 660 °C at 1 atm pressure [24]. When Unde et al. tested the Al₂O₃ catalyst through RWGS reaction, they discovered that the CO₂ to CO conversion equilibrium was reached at a high temperature of 900 °C. Reaction was controlled kinetically between 300 and 700 °C, and thermodynamically above this temperature range [26]. As a result, production of active RWGS catalysts operated at low-temperature with higher CO selectivity and limited CH₄ production was required. Insight into the mechanisms of CO production is also vital for rational catalyst design in such processes. Various reaction routes could lead to various kinetic parameters and selectivity variations for CO₂ hydrogenation [27].



According to the concept of microscopic reversibility and the fact that the RWGS reaction is typically carried out at equilibrium, the active catalysts in the water gas shift (WGS) process are also effective in the RWGS reaction, but may be under different reaction conditions, suggesting that similar catalysts should enhance both reactions [28]. Some typical features of WGS catalysts include the presence of oxygen vacancies, the strength at which CO can be adsorbed, and activity for dissociation of water [29]. In the earlier study, a thorough overview of the most recent advancements of catalysts utilized in low-temperature WGS reactions is presented [30]. In various CO₂ conversion processes, many types of catalysts have been used, including oxide-supported metal catalysts and oxide catalysts in which cerium oxide (CeO₂) has had a key role [30][31]. CeO₂ is a typical rare earth metal oxide with a face-centered cubic (FCC) fluorite structural pattern, and has oxygen storage capacity (OSC) and a number of intriguing features that can be exploited to improve catalytic efficiency [28][32]. In comparison to other reducible oxides, oxygen vacancies on the surface of CeO₂ are more easily formed during the reduction process owing to its unique electron arrangement [33]. Besides, the reversible redox pair Ce³⁺/Ce⁴⁺ and the acid basic surface properties of CeO₂ are effectively leading to its broader catalytic application [34]. It was found that the reducibility of ceria had an inverse connection with the bimetallic cluster promoted local electronic band, which caused the stability of germinal OH groups and was assumed to be the reason for higher WGS activity [35]. Besides, the RWGS reaction has been reported to work well with noble metal-loaded CeO₂ catalysts [36]. In a comparative study, Castao et al. looked at the efficiency of platinum and gold catalysts on ceria supports [37]. Transition metals supported on CeO₂ also have greater RWGS activity than metals supported on non-reducible supports. Moreira et al. investigated the sorption-accelerated WGS process at low temperature (125–295 °C) over Cu-CeO₂/HTlc catalysts; Cu supported on polyhedral nanoparticle-sized ceria displayed a high conversion of 87.6% [38]. Comparing the performances of 1.7% Pt-CeO₂ and Pt-Al₂O₃ at 573 K in WGS reaction, Porosof and Chen examined the amount of CO uptake as an indicator of the dispersion of Pt metal. They found out that the amount of CO uptake using Pt-CeO₂ is ~5.7 times higher than that on Pt-Al₂O₃ [39].

2. Preparation Methods

The method of catalyst preparation determines the metal-support interaction and morphological properties of the final catalysts that considerably impact the performance of the catalysts. The impact of different preparation procedures of 1 wt.% Ni-CeO₂, e.g., co-precipitation (CP), deposition–precipitation (DP), and impregnation (IM) approaches, on the physicochemical and catalytic characteristics in the RWGS reaction was explored by Luhui et al. [40]. The Ni-CeO₂-CP catalyst achieved the highest conversion rate in the RWGS reaction when compared to the Ni-CeO₂-DP and Ni-CeO₂-IM catalysts; however, the CO selectivity followed the order: Ni-CeO₂-IM > Ni-CeO₂-CP > Ni-CeO₂-DP. As confirmed by TPR analysis, an integration of numerous oxygen vacancies and broadly dispersed small NiO particles was considered to be the reason for the outstanding performance of the Ni-CeO₂-CP catalyst in terms of high activity and good selectivity. This suggests that more nickel ions were integrated into the CeO₂ lattice to develop a solid solution. The Ni-CeO₂-DP catalyst has only a limited number of oxygen vacancies in comparison to the Ni-CeO₂-CP catalyst, which results in low RWGS selectivity. It was proposed that the RWGS selectivity was strongly influenced by the oxygen vacancies. It is believed that the solid solution of Ce_xNi_yO is produced when the Ni²⁺ ions are inserted into the ceria lattice to substitute certain Ce⁴⁺ cations [40]. Oxygen vacancies are produced by the lattice distortion and charge imbalance that occur within the CeO₂

structure [41][42]. Several reports have indicated that precipitated ceria-based catalysts have distinct properties depending on the precipitants used, which significantly influence structural properties and catalytic performance [43][44][45][46][47][48]. In other work by the same group, Luhui et al. used the CP method to make a range of Ni-CeO₂ catalysts using Na₂CO₃, NaOH, as well as a combination of precipitants (Na₂CO₃:NaOH; 1:1 ratio) in order to investigate their catalytic efficacy in the RWGS reaction [49]. According to the structural characterization findings, the catalyst developed by the mixed precipitating agents (Na₂CO₃:NaOH; 1:1 ratio) exhibited the highest oxygen vacancies along with high Ni particle dispersion, resulting in the highest catalytic activity for the corresponding catalyst, whereas the precipitants' catalytic selectivity for CO were ranked as: NaOH > Na₂CO₃ > Na₂CO₃:NaOH = 1:1 [49]. The technique used to synthesize the CeO₂ catalyst has a substantial impact on its structure, and the structure of the synthesized catalysts can greatly influence the catalytic performance in the CO₂ RWGS reaction [50]. Hard-template (HT), complex (CA), and precipitation strategies (PC) were used to synthesize CeO₂ catalysts with various structures, and their efficiency in the CO₂ RWGS reaction was examined by Dai et al. [50]. The Ce-HT catalyst had the greatest CO₂ RWGS reaction activity due to its porous structure (TEM), high specific surface area of 144.9 m².g⁻¹ (BET), and abundance of oxygen vacancies; Ce-HT > Ce-CA > Ce-PC is the temperature sequence in which the catalysts reduce in the presence of H₂ at low temperatures (H₂-TPR) [50]. Xiaodong et al. carried out the RWGS reaction over Pt-CeO₂ catalysts at temperatures between 200 and 500 °C under atmospheric pressure and various pretreatment conditions using the co-precipitated technique [51]. The samples were represented as PC-M-N, where PC stands for the co-precipitated 1%Pt-CeO₂ catalyst and M and N stand for the calcination and reduction temperatures of the samples, respectively, [51]. The catalyst prepared at a lower calcination temperature (PC-500-400) demonstrated a more favorable catalytic performance than the others due to its high Pt dispersion [51]. In another study, Ronda-Lloret et al. investigated the use of metal organic frameworks (MOFs) as precursors instead of merely using the traditional wet impregnation (WI) method in the production of CuO_x-CeO₂ catalysts [52]. After impregnating Cu-MOF using a ceria precursor, they flash-pyrolized (PF) the impregnated MOF applying distinctive conditions and procedures and compared the performances in the RWGS reaction with the WI synthesis technique finding that the MOF-derived catalyst outperformed the other catalyst [52]. Throughout the thermal decomposition procedure, the metal ions in MOFs are transformed into metallic or metal oxide nanoparticles, while the organic linkers produce carbonaceous formations which can function as supports and promote active phase distribution [53]. As Ronda-Lloret et al. concluded, by changing the pyrolysis environment, an oxidizing environment may be produced that prevents sintering and keeps copper oxidized during decomposition. Using air in the decomposition process causes the creation of copper oxide compounds that sinter with more difficulty than the metallic copper. This promotes the interaction with the ceria support, which improves its catalytic behavior. Thus, by utilizing air, highly dispersed CuO on CeO₂ can be created that is readily reducible and exhibits strong interactions with the ceria [52].

3. Shape and Crystal Face Effect

The form and exposed crystal face of catalysts have a major impact on RWGS reaction activity since they may control the adsorption and desorption energies of precursors in the reaction process [54][55][56]. Thus, the efficiency of CeO₂ supported catalysts can be modified by conducting experiments with various morphologies. The RWGS reaction was studied by Kovacevic et al. over cerium oxide catalysts of various morphologies: cubes, rods, and particles [57]. Using TPR they found that surface oxygen is less removable in the case of nanoshapes with a high concentration of oxygen vacancies and, compared to rods and particles, cerium oxide cubes had twice more activity per surface area. The stronger intrinsic reactivity of (100) crystal planes encapsulating cubes, as opposed to less intrinsically reactive (111) facets exhibited in rods and particles, results in enhanced catalytic activity of ceria cubes in RWGS [57]. In another study, Lin et al. found that under similar conditions and the same active metal, the CeO₂(110) surface has substantially more activity than the CeO₂(111) surface, indicating that the ceria support performance is facet-dependent [58]. According to their study, once Cu particles are loaded onto the CeO₂-Nanorod (NR) and CeO₂-Nanosphere (NS) surfaces, the NR sample exhibits greater RWGS reaction activity. This is mostly due to the increased feasibility of CO₂ dissociative activation and the generation of active bidentate carbonate and formate intermediates over CeO₂(110) [58]. Liu et al. used RWGS to compare crystal plane reactive activity in three nano-CeO₂s with varied exposed planes [59]. The overall order of RWGS reactive efficiency of the three studied CeO₂ shapes was ceria nanocube (NC) > ceria-NR > ceria-nanooctahedra (NO) [59]. It is well established that oxygen vacancies formation on ceria (100) or (110) consume less energy than creating them on ceria (111) [60][61]. As a result, the ceria (100) and (110) planes seem to be more attractive choices for catalyzing processes that involve an oxygen cycle with adsorbates [59]. This could be the main reason why the ceria-NC exposed (100) plane had the best CO₂ conversion and selectivity.

Zhang et al. developed self-assembled CeO₂ with 3D hollow nanosphere (hs) (111), nanoparticle (np) (111), and nanocube (nc) (200) morphologies that were employed to support Cu particles [62]. Owing to the large levels of active oxygen vacancy sites, the Cu-CeO₂-hs(111) exhibited the greatest RWGS catalytic activity among the studied catalysts

[62]. Konsolakis et al. looked into the influence of the active phase type and ceria nanoparticle support morphology (NR or NC) on the physicochemical characteristics and CO₂ hydrogenation capability of M-CeO₂ (M = Co or Cu) composites at 1 atm [63]. Regardless of support structure, CO₂ conversion was reported to follow the following order: Co-CeO₂ > Cu-CeO₂ > CeO₂ with the Cu-CeO₂ sample being far more selective toward CO than Co-CeO₂. The Co catalysts supported on NC ceria demonstrated slightly higher catalytic activity than Co supported on rod-like forms, highlighting the importance of support morphology in addition to the choice of metal element; for Cu-based samples and bare CeO₂, the pattern was the opposite [63].

4. Metal–Support Interactions

Activation of catalysts by pretreatment at high-temperature in the presence of hydrogen is often adopted to reduce the oxide nanoparticles and generate oxygen vacancies on the reducible support surface; however, such activation procedures can develop greater interactions between metal nanoparticles and the support, which has been reported to impact catalytic activity in varying ways: positively [64], negatively [65], or in some cases insignificantly [66]. The strong metal–support interaction (SMSI) phenomenon, which typically develops in metals and reducible oxides subjected to high reduction temperature, is one such case [67]. The type of the support [68], metal composition [69], and catalyst synthesis procedure can all influence metal–support interaction (MSI) [70]. According to Goguet et al., the major active site in the RWGS reaction over Pt-CeO₂ catalyst is the interface among Pt and CeO₂ and the reducible site of CeO₂, which is created by the SMSI effect of Pt and CeO₂ [71].

SMSI between Cu species and CeO₂ helps in boosting the reducibility and stability of associated catalysts, which is favorable for catalytic reduction processes [72]. The results of a study by Zhou et al. showed that the H₂ reduction at 400 °C can create oxygen vacancies and active Cu⁰ species as active sites in Cu-CeO₂ catalysts [73]. The SMSI phenomenon allows electrons to move from Cu to Ce on its surface, forming the Ce³⁺-O_v-Cu⁰ and Cu⁰-CeO_{2-δ} interface structures that increase the adsorption and activation of the reactant in RWGS reaction. The results suggested that the Cu-CeO₂ catalyst with 8 wt.% Cu had the best CO₂ conversion yield. The full synergistic interaction between the active species via Ce³⁺-oxygen vacancy-Cu⁰ was attributed to its high catalytic activity in the RWGS process [73].

Aitbekova et al. designed the 2.6 nm Ru equally distributed on Al₂O₃, TiO₂, and CeO₂ supports and tested in a CO₂ reduction process [74]. Ru catalysts supported on TiO₂ and CeO₂ were significantly more active than those supported on Al₂O₃, but CH₄ was the predominant product in all cases. Nonetheless, they reported that moderate oxidation of the catalyst at a temperature of 230 °C followed by low temperature reduction (230 °C), named as OX-LTR, leads to the Ru particles' re-dispersion on CeO₂, giving a nearly complete switching of product selectivity from methane to CO, indicating that a weaker adsorption of CO on the single RuO_x site is likely to result in increased selectivity. As they stated in their research, such re-dispersion appears only slightly in Al₂O₃- and TiO₂-supported Ru, probably due to the lower Al₂O₃ and TiO₂ and RuO_x interaction as compared to the CeO₂ support with RuO_x. Moreover, a light oxidation of the catalysts at 230 °C coupled with a high reduction temperature of 500 °C, named as OX-HTR, favored the formation of SMSI in the case of Ru-TiO₂; however, the Ru-CeO₂ catalysts (both OX-LTR and OX-HTR) exhibited fairly similar rates, implying the effect of SMSI is negligible for CeO₂-supported Ru materials under the CO₂ hydrogenation conditions investigated [74]. Similar conclusions were derived by Tauster et al. in a separate study [75].

A capping layer encircling the supported nanoparticles is commonly observed as evidence of the impact [76]. The existence of such an action, on the other hand, could be linked to charge transfer across metallic nanoparticles and the oxide support [77]. For example, Figueiredo et al. synthesized Cu_xNi_{1-x}-CeO₂ (x = 0.25, 0.35 and 60) nanoparticles for use in the RWGS reaction and investigated the SMSI influence on CO₂ dissociation reaction by exploring the nanoparticles' electrical and structural features and discovered the reactivity of nanoparticles was proportional to the Cu content on the surface with Cu-rich ones having a negative impact on the CO₂ dissociation reactivity [78]. According to their experimental results, through the reduction treatment, the SMSI effect does not actually impact nanoparticles synthesized with low Cu amounts. The SMSI situation caused the support's capping layer that surrounds the nanoparticle surface to cover the catalytic active spots on the surface of the nanoparticle, leading to a decrease in the reactivity of CO₂ dissociation [78].

The area of the CO₂ desorption peak and the number of CO₂ adsorption active sites present on the surface of the relevant catalyst are invariably connected. By increasing Cu loading, the peak regions for the ε peak exhibited a volcano pattern, reaching their highest on the 8Cu/CeO_{2-δ} catalyst. This was explained in their work by the fact that increasing Cu loading (8%) led to a greater number of Cu- CeO_{2-δ} junctions and encouraged strong MSI. Nonetheless, at larger Cu loadings (>8%), a portion of the surface active sites may be coated by an extreme amount of Cu species [73]. When it comes to the peak φ, the peak regions initially start to increase, up to Cu loading of 10%, and then continue to decrease. This was

explained by the fact that at lower Cu loadings up to 10%, the catalysts' high specific surface areas enable CO₂ molecules to adsorb on their surfaces, whereas at larger Cu loadings (above 10%), the catalysts' active sites are reduced as a result of the evident decrease in specific surface areas [73].

5. Active Metal Loading

The influence of the catalysts' composition has been investigated in many studies. Lloret et al. designed catalysts with two different Cu concentrations and two different quantities of ceria precursor, aiming to have two distinct molar ratios of 20Cu:80Ce and 40Cu:60Ce with two different decomposition methods: pyrolysis (P), and PF [52]. It was revealed that samples with a higher Cu level have weak catalytic activity, whereas catalysts with a lower Cu content have better catalytic behavior in the RWGS process [52]. It is interesting to note that the ceria crystal size is smaller in the catalyst with higher ceria content (lower Cu), and copper dispersion is reduced when there is a large copper loading. According to the TPR results, hydrogen consumption was higher and peaked at lower temperatures in the sample with less Cu. A high Cu content needed the degradation of a greater quantity of HKUST-1, creating a more reducing environment. Therefore, if higher Cu content is there, additional MOFs are needed to break down to adjust to the reducing environment [52]. The impact of metal nanoparticle concentration on CeO₂-supported Pt and Ru catalysts with metal contents of 1, 5, and 10% on CeO₂ has been investigated by Einakchi et al. [79]. Ru and Pt catalysts are likely to have lower metal dispersion at 10 wt.% when compared to metal loadings of 1 wt.%. The high catalytic performance of Pt-CeO₂ was found to be linked with metal loading and particularly sensitive to metal dispersion, with 1 wt.% Pt displaying the optimum catalytic performance. Unlike Pt-CeO₂, no correlation was identified between Ru catalyst RWGS activity and metal loading (Ru dispersion); nonetheless, 5 wt.% Ru metal was proven to be the best loading for Ru-CeO₂ catalysts [79]. In another study, Wang et al. prepared Co-CeO₂ catalysts with different cobalt concentrations (0, 1, 2, 5, 10%) using the CP method employed in the RWGS reaction [80]. The findings revealed that the sample with 2% Co on CeO₂ support showed highly dispersed Co₃O₄ on CeO₂ surface displaying a strong MSI that resulted in an outstanding RWGS catalytic efficiency in terms of activity, CO selectivity, and minimal carbon deposition. Nevertheless, bulk Co₃O₄ with bigger particle size generated in catalysts having high Co content (5% and 10%) lead to considerably higher carbon deposition and enhanced by-product CH₄ generation throughout the process. Their results suggested that for the RWGS reaction, widely dispersed Co which is reduced from highly distributed Co₃O₄ on CeO₂ support, ought to be a major active material, whereas solid Co that has a large particle size could be the main active component for methanation as well as carbon deposition [80]. The same group in another study investigated the effect of the content of cobalt supported on CeO₂ prepared by a colloidal solution combustion technique to form mesoporous catalysts (Co-CeO₂-M) and examined their activity and selectivity toward RWGS reaction and then compared the optimum Co amount sample with the same catalyst prepared by IM and CP [81]. The catalytic analyses revealed that the mesoporous 5% and 10%Co-CeO₂ catalyst had high activity in the RWGS reaction; however, 10%Co-CeO₂ was less selective to CO formation than the 5%Co-CeO₂ one. Nonetheless, both had good stability over a 10-h period at 600 °C. Moreover, the activity and selectivity of 5% Co-CeO₂-M was higher than the 5% Co-CeO₂-IM and 5%Co-CeO₂-CP catalysts. They concluded that the superior catalytic performance of the 5%Co-CeO₂-M catalyst was owing to its unique mesoporous configuration, in which the Co particle is dispersed throughout the pore wall and is in close contact to small CeO₂ particles [81]. When defining the optimal catalyst in terms of activity and selectivity, metal dispersion is not the only factor to consider; the nature of the support also plays an important role. According to research by Jurkovic et al. on various supports for Cu-based catalysts, the supports with the greatest Cu dispersion were Al₂O₃ (77.7%) followed by ZrO₂ (73.6%), CeO₂ (67.6%), TiO₂ (66.3%), and SiO₂ (36.2%) [82]. Nevertheless, the alumina support was found to have the highest reported catalytic activity, followed by ceria, titania, silica, and zirconia. Ceria was ranked by TPR as the second-best support among the studied group, while having the third-best Cu dispersion, most likely because of its reducibility and capacity to hold oxygen [82]. Moreover, according to the literature, there is a direct correlation between the catalysts' activity and acid-base properties [83]. According to Pino et al., the synergistic interaction of Ni and La₂O₃ on a La₂O₃ doped Ni-CeO₂ catalyst boosted catalytic activity because of the creation of a basic site and Ni dispersion improvement [84]. Therefore, it can also be concluded that improving basicity of a catalyst might facilitate CO₂ adsorption [85]. According to the research of Jurkovic et al., Al₂O₃ is a frequently used irreducible support with good performance, where its modest acidity could be a likely contributing factor [82][85].

6. Metal Size Effect

The RWGS reaction is sensitive to the structure of the supported catalysts, and the size of the attached metal active sites that influence the adsorption, intermediate formation and desorption of the products [86]. Reducing the metal particle size may improve MSI by generating a larger metal-support interface, leading to positively increasing the RWGS reaction activity. Indeed, due to the SMSI effect, more oxygen atoms should be attached to the metal surface when the particle size decreases [87]. For example, Li et al. developed a 5% Ir-CeO₂ catalyst including an Ir particle size of around 1 nm,

and a 0.7% Ir-CeO₂ catalyst with atomic dispersion of Ir [88]. Even though the dominant product of CH₄ was produced by an Ir-CeO₂ catalyst with large Ir particles (>2.5 nm), CO was produced mainly by the 5% and 0.7% Ir-CeO₂ catalysts when Ir particle size was less than 1 nm, and the catalytic activity per mole of Ir increased. They also discovered that due of the intense interaction with CeO₂, 1 nm Ir particles and atomically dispersed Ir get partially oxidized, but large Ir particles, more than 2.5 nm, are mostly reduced. As a result, they concluded that the primary active site for a RWGS reaction is partly oxidized Ir that engages extensively with CeO₂ support regardless of Ir particles or atomically dispersed Ir atoms [88]. Metal active sites distributed on an atomic level add more to the CO product than metal clusters at a 3D level [89]. In a study, Zhao et al. produced Pt-CeO₂ catalysts with various Pt sizes to test the influence of size on CO selectivity in the RWGS reaction [90]. Three Pt-CeO₂ catalysts were produced using CeO₂ nanorods, including atomically dispersed Pt species as well as Pt clusters or particles of two different sizes (2.1 and 5.2).

Lu et al. developed mesoporous CeO₂ (surface area = 100 m² g⁻¹) as well as NiO-CeO₂ with large surface areas, narrow pore size dispersion, and homogeneous mesopores (intercrystallite voids) [91]. According to the results, with increasing temperature and NiO quantity, the CO₂ conversion rate in RWGS reaction increased. As for CO selectivity, when less than 3 wt.% NiO was used, NiO particles monodispersed in mesoporous CeO₂ resulting in a complete CO₂ conversion to CO which was irrespective of temperature. For more than 3.5 wt.%, due to NiO particle aggregation, 100% CO selectivity was improbable below 700 °C [91]. Wang et al. studied the effect of CeO₂ on RWGS in comparison to In₂O₃ [92]. The surface areas of the In₂O₃-CeO₂ catalysts enhanced compared to pure In₂O₃; as the CeO₂ content increased, the size of the In₂O₃ particles in the In₂O₃-CeO₂ samples reduced and the dispersion of In₂O₃ particles in the In₂O₃-CeO₂ increased. Besides, additional oxygen vacancies were formed, which in turn enhanced the dissociative hydrogen adsorption and increased the quantity of bicarbonate species produced by activated CO₂ adsorption [92].

7. Effect of Adding CeO₂ as a Reducible Transition Metal Oxide Promoter

The inclusion of a cerium oxide as a promoter can affect CO₂ adsorption and activation, as well as the activity and selectivity of the RWGS process [93][94]. Yang et al. showed in their work how adding ceria to alumina support (CeO₂-Al₂O₃) helped in lowering acidity of Ni-based catalysts, which also minimized carbon deposition [95]. The researchers concluded that their findings were mostly due to two aspects occurring together: (1) CeO₂, as a promoter here, reduced the Ni-Al₂O₃ connection, leading to an increase in Ni particle reducibility, owing to the generated Ni-promoter interaction, and (2) because of its intrinsic redox capabilities, CeO₂ offered additional oxygen mobility to the catalysts [96]. In another study by Lee et al., a set of Pt-CeO₂-TiO₂ catalysts were impregnated with different support combinations ranging from 0 to 20% to evaluate the influence of varied CeO₂/TiO₂ ratio on catalytic activity during RWGS reaction [97]. Accordingly, increasing CeO₂ loading improved the catalytic activity of Pt-impregnated catalysts, the Pt-20%CeO₂-TiO₂ sample showing the highest CO₂ conversion. Based on their analysis, by substituting TiO₂ with CeO₂, the lattice and pore configuration changed in favor of more CO₂ conversion in RWGS reaction [97]. With the aim of improving adsorption and activation of CO₂ on Ga₂O₃, Zhao et al. used CeO₂ as a promoter with an optimum Ga:Ce ratio of 99:1 and employed RWGS reaction as a test reaction and indicator for the catalytic performance of the resultant samples [98]. The results showed the positive performance of CeO₂-Ga₂O₃ due to the fact that the inclusion of CeO₂ increases the production of bicarbonate species in CO₂ adsorption, which is thermodynamically more advantageous [98]. The same catalytic system was studied by Dai et al., where the gel sol-gel process was used to create a variety of Ga₂O₃-CeO₂ composite oxide catalysts with various Ga₂O₃ and CeO₂ ratios [99]. When compared to pure Ga₂O₃ and pure CeO₂, the composite oxide catalysts had smaller particles and showed high CO selectivity in the RWGS process. It was discovered that Ga₂O₃ has distinct reaction intermediates from CeO₂ and Ga₂O₃-CeO₂, making it easier to create methane in high H₂ conditions, whereas CeO₂ promotes CO selectivity. In a Ga₂O₃ to CeO₂ ratio of 3:1, composite oxide showed the greatest activity. This is mostly due to the creation of the Ga_xCe_yO_z solid solution phase and the development of additional active sites that result in an increased number of oxygen vacancies, which facilitate CO₂ adsorption and activation. Moreover, it was found that GaCe composite oxides have a more homogeneous mesoporous structure and a greater pore volume, making mass transport in reactions easier [99]. In contrast, there are a few cases in which once ceria was introduced to a catalytic system, CO selectivity improved but CO₂ conversion was slightly decreased [100]. Galvita et al., for example, developed a Fe₂O₃-CeO₂ composite and discovered that incorporating ceria to iron oxide increased solid solution stability but reduced CO production capabilities [101].

On the other hand, when a non-reducible transition metal oxide is used as a promoter for M-CeO₂ catalysts, more oxygen vacancies can emerge during the reduction process [102]. For example, more thermally stable support can be developed by a mixed framework of Al₂O₃-CeO₂ which offers a broad surface for optimum active phase dispersion and enables the development of oxygen vacancies on the surface throughout the catalytic reaction to improve catalytic performance [103].

Zonetti et al. and Wenzel et al. showed that adding Zr to the CeO₂ lattice improved its ability to create oxygen vacancies as well as its thermal stability, which is a desirable feature of catalytic systems ^{[104][105]}.

8. Bimetallic Effect

Reports indicate that bimetals, where a second metal is introduced along with the primary active metal, can be used to help boost the catalytically active phase ^[106]. Evidently in many systems, bimetallic compounds have outperformed their individual components ^[107]. Furthermore, the generation of metal carbide (coke precursor) could be prevented due to the electrical effect caused by metal–metal interactions, resulting in less deactivation ^[108]. Yang et al. showed how the inclusion of a second element (Cr or Fe) can positively affect the reducibility of monometallic Ni-based catalysts (Ni-CeAl) ^[95]. The addition of Fe to the Ni-CeAl catalyst system can increase the reducibility of Ni- to 95% compared to 93% for the Ni-CeAl catalyst ^[95]. Chen et al. synthesized a Cu-Fe bimetallic phase loaded on CeO₂ and evaluated its performance for RWGS reaction at temperatures ranging from 450 to 750 °C at 1 atm. The efficiency of the iron-containing copper-based catalyst was greatly increased over that of the catalyst without iron, and CO₂ conversion nearly approached theoretical levels. The bimetallic CeO₂-supported catalyst was shown to have high selectivity, stability, with no secondary reactions, and no carbon deposition on the catalyst surface after the process ^[109]. In contrast, Li et al. used CuIn bimetallic catalysts for the RWGS reaction, demonstrating that the promotional impact of In on Cu is support dependent ^[110]. The CO₂ conversion of the CuIn-ZrO₂ catalyst was higher by far than the Cu-ZrO₂ catalyst; however, the CO₂ conversion of CuIn-CeO₂ was considerably lower than Cu-CeO₂. The cause of the support-sensitivity of RWGS activity was further discovered through systematic analysis. Cu and In combined to form CuIn alloys on the ZrO₂ support, which allowed CO₂ to be activated by oxygen vacancies from partially reduced In₂O₃, whereas, Cu and In were found as metallic Cu and In₂O₃ on the CeO₂ support, respectively. The addition of In prevented Cu dispersion and the development of oxygen vacancies on CeO₂, resulting in lower RWGS activity ^[110].

References

1. Yang, X.; Su, X.; Chen, X.; Duan, H.; Liang, B.; Liu, Q.; Liu, X.; Ren, Y.; Huang, Y.; Zhang, T. Promotion effects of potassium on the activity and selectivity of Pt/zeolite catalysts for reverse water gas shift reaction. *Appl. Catal. B Environ.* 2017, 216, 95–105.
2. Ebrahimi, P.; Kumar, A.; Khraisheh, M. Thermodynamic assessment of effect of ammonia, hydrazine and urea on water gas shift reaction. *Int. J. Hydrogen Energy* 2020, 47, 3237–3247.
3. Sasol ECOFT and Deutsche Aircraft join forces to accelerate power-to-liquid (PTL) aiming for carbon-neutral flight. *Focus Catal.* 2022, 2022, 4.
4. Liu, X.; Pajares, A.; Matienzo, D.D.C.; de la Piscina, P.R.; Homs, N. Preparation and characterization of bulk MoXC catalysts and their use in the reverse water-gas shift reaction. *Catal. Today* 2020, 356, 384–389.
5. Centi, G.; Perathoner, S. Opportunities and prospects in the chemical recycling of carbon dioxide to fuels. *Catal. Today* 2009, 148, 191–205.
6. Aresta, M. *Carbon Dioxide as Chemical Feedstock*; John Wiley & Sons: Hoboken, NJ, USA, 2010.
7. Ueckerdt, F.; Bauer, C.; Dirnacher, A.; Everall, J.; Sacchi, R.; Luderer, G. Potential and risks of hydrogen-based e-fuels in climate change mitigation. *Nat. Clim. Chang.* 2021, 11, 384–393.
8. Olah, G.A.; Goeppert, A.; Prakash, G.S. Chemical recycling of carbon dioxide to methanol and dimethyl ether: From greenhouse gas to renewable, environmentally carbon neutral fuels and synthetic hydrocarbons. *J. Org. Chem.* 2009, 74, 487–498.
9. Sterner, M. *Bioenergy and Renewable Power Methane in Integrated 100% Renewable Energy Systems. Limiting Global Warming by Transforming Energy Systems: Limiting Global Warming by Transforming Energy Systems*; Kassel University Press GmbH: Hesse, Germany, 2009; Volume 14.
10. Pastor-Pérez, L.; Baibars, F.; Le Sache, E.; Arellano-Garcia, H.; Gu, S.; Reina, T.R. CO₂ valorisation via reverse water-gas shift reaction using advanced Cs doped Fe-Cu/Al₂O₃ catalysts. *J. CO₂ Util.* 2017, 21, 423–428.
11. Galván, C.Á.; Schumann, J.; Behrens, M.; Fierro, J.L.G.; Schlögl, R.; Frei, E. Reverse water-gas shift reaction at the Cu/ZnO interface: Influence of the Cu/Zn ratio on structure-activity correlations. *Appl. Catal. B Environ.* 2016, 195, 104–111.
12. Sheehan, S.W. Electrochemical methane production from CO₂ for orbital and interplanetary refueling. *Iscience* 2021, 24, 102230.

13. Xu, X.D.; Moulijn, J.A. Mitigation of CO₂ by chemical conversion: Plausible chemical reactions and promising products. *Energy Fuels* 1996, 10, 305–325.
14. Kwak, J.H.; Kovarik, L.; Szanyi, J.N. Heterogeneous catalysis on atomically dispersed supported metals: CO₂ reduction on multifunctional Pd catalysts. *ACS Catal.* 2013, 3, 2094–2100.
15. Yasuda, T.; Uchiage, E.; Fujitani, T.; Tominaga, K.-I.; Nishida, M. Reverse water gas shift reaction using supported ionic liquid phase catalysts. *Appl. Catal. B Environ.* 2018, 232, 299–305.
16. Wender, I. Reactions of synthesis gas. *Fuel Process. Technol.* 1996, 48, 189–297.
17. ExxonMobil unveils tech for methanol-to-SAF. *Focus Catal.* 2022, 2022, 6.
18. Kumar, A.; Mohammed, A.A.; Saad, M.A.; Al-Marri, M.J. Effect of nickel on combustion synthesized copper/fumed-SiO₂ catalyst for selective reduction of CO₂ to CO. *Int. J. Energy Res.* 2022, 46, 441–451.
19. De Miranda, P.E.V. Chapter 5.3.3—Application of Hydrogen by Use of Chemical Reactions of Hydrogen and Carbon Dioxide. In *Science and Engineering of Hydrogen-Based Energy Technologies*; de Miranda, P.E.V., Ed.; Academic Press: Cambridge, MA, USA, 2019; pp. 279–289.
20. Stangeland, K.; Kalai, D.; Li, H.; Yu, Z. CO₂ methanation: The effect of catalysts and reaction conditions. *Energy Procedia* 2017, 105, 2022–2027.
21. Nityashree, N.; Price, C.; Pastor-Perez, L.; Manohara, G.; Garcia, S.; Maroto-Valer, M.M.; Reina, T. Carbon stabilised saponite supported transition metal-alloy catalysts for chemical CO₂ utilisation via reverse water-gas shift reaction. *Appl. Catal. B Environ.* 2020, 261, 118241.
22. Dias, Y.R.; Perez-Lopez, O.W. Carbon dioxide methanation over Ni-Cu/SiO₂ catalysts. *Energy Convers. Manage.* 2020, 203, 112214.
23. Elseragawy, O.Y.; Hoadley, A.; Patel, J.; Bhatelia, T.; Lim, S.; Haque, N. Thermo-economic analysis of reverse water-gas shift process with different temperatures for green methanol production as a hydrogen carrier. *J. CO₂ Util.* 2020, 41, 101280.
24. Kaiser, P.; Unde, R.B.; Kern, C.; Jess, A. Production of liquid hydrocarbons with CO₂ as carbon source based on reverse water-gas shift and Fischer-Tropsch synthesis. *Chem. Ing. Tech.* 2013, 85, 489–499.
25. York, A.P.; Xiao, T.C.; Green, M.L.; Claridge, J.B. Methane oxyforming for synthesis gas production. *Catal. Rev.* 2007, 49, 511–560.
26. Unde, R.B. Kinetics and Reaction Engineering Aspects of Syngas Production by the Heterogeneously Catalysed Reverse Water Gas Shift Reaction; Universitaet Bayreuth: Bayreuth, Germany, 2012.
27. Wu, H.; Chang, Y.; Wu, J.; Lin, J.; Lin, I.; Chen, C. Methanation of CO₂ and reverse water gas shift reactions on Ni/SiO₂ catalysts: The influence of particle size on selectivity and reaction pathway. *Catal. Sci. Technol.* 2015, 5, 4154–4163.
28. Ebrahimi, P.; Kumar, A.; Khraisheh, M. Combustion synthesis of copper ceria solid solution for CO₂ conversion to CO via reverse water gas shift reaction. *Int. J. Hydrogen Energy* 2022, in press.
29. Ammal, S.C.; Heyden, A. Origin of the unique activity of Pt/TiO₂ catalysts for the water–gas shift reaction. *J. Catal.* 2013, 306, 78–90.
30. Ebrahimi, P.; Kumar, A.; Khraisheh, M. A review of recent advances in water-gas shift catalysis for hydrogen production. *Emergent Mater.* 2020, 3, 881–917.
31. Boaro, M.; Colussi, S.; Trovarelli, A. Ceria-based materials in hydrogenation and reforming reactions for CO₂ valorization. *Front. Chem.* 2019, 7, 28.
32. Ebrahimi, P.; Kumar, A.; Khraisheh, M. Analysis of combustion synthesis method for Cu/CeO₂ synthesis by integrating thermodynamics and design of experiments approach. *Results Eng.* 2022, 15, 100574.
33. Ishito, N.; Hara, K.; Nakajima, K.; Fukuoka, A. Selective synthesis of carbon monoxide via formates in reverse water–gas shift reaction over alumina-supported gold catalyst. *J. Energy Chem.* 2016, 25, 306–310.
34. Trovarelli, A. Catalytic properties of ceria and CeO₂-containing materials. *Catal. Rev.* 1996, 38, 439–520.
35. Yeung, C.M.; Tsang, S.C. A study of co-precipitated bimetallic gold catalysts for water–gas shift reaction. *Catal. Commun.* 2008, 9, 1551–1557.
36. Chang, K.; Zhang, H.; Cheng, M.-J.; Lu, Q. Application of ceria in CO₂ conversion catalysis. *ACS Catal.* 2019, 10, 613–631.
37. Castaño, M.G.; Reina, T.R.; Ivanova, S.; Centeno, M.; Odriozola, J.A. Pt vs. Au in water–gas shift reaction. *J. Catal.* 2014, 314, 1–9.

38. Moreira, M.N.; Ribeiro, A.M.; Cunha, A.F.; Rodrigues, A.E.; Zabilskiy, M.; Djinić, P.; Pintar, A. Copper based materials for water-gas shift equilibrium displacement. *Appl. Catal. B Environ.* 2016, 189, 199–209.
39. Porosoff, M.D.; Chen, J.G. Trends in the catalytic reduction of CO₂ by hydrogen over supported monometallic and bimetallic catalysts. *J. Catal.* 2013, 301, 30–37.
40. Luhui, W.; Hui, L.; Yuan, L.; Ying, C.; Shuqing, Y. Influence of preparation method on performance of Ni-CeO₂ catalysts for reverse water-gas shift reaction. *J. Rare Earths* 2013, 31, 559–564.
41. Li, Y.; Zhang, B.; Tang, X.; Xu, Y.; Shen, W. Hydrogen production from methane decomposition over Ni/CeO₂ catalysts. *Catal. Commun.* 2006, 7, 380–386.
42. Yisup, N.; Cao, Y.; Feng, W.-L.; Dai, W.-L.; Fan, K.-N. Catalytic oxidation of methane over novel Ce–Ni–O mixed oxide catalysts prepared by oxalate gel-coprecipitation. *Catal. Lett.* 2005, 99, 207–213.
43. Huang, Y.; Wang, A.; Li, L.; Wang, X.; Su, D.; Zhang, T. “Ir-in-ceria”: A highly selective catalyst for preferential CO oxidation. *J. Catal.* 2008, 255, 144–152.
44. Li, L.; Song, L.; Wang, H.; Chen, C.; She, Y.; Zhan, Y.; Lin, X.; Zheng, Q. Water-gas shift reaction over CuO/CeO₂ catalysts: Effect of CeO₂ supports previously prepared by precipitation with different precipitants. *Int. J. Hydrogen Energy* 2011, 36, 8839–8849.
45. Yongyi, H.; Qibiao, L.; Yongzhao, W.; Yongxiang, Z. Selective catalytic dehydration of 1, 4-butanediol to 3-buten-1-ol over CeO₂ with different morphology. *Chin. J. Catal.* 2010, 31, 619–622.
46. Dong, X.-F.; Zou, H.-B.; Lin, W.-M. Effect of preparation conditions of CuO–CeO₂–ZrO₂ catalyst on CO removal from hydrogen-rich gas. *Int. J. Hydrogen Energy* 2006, 31, 2337–2344.
47. Xue, L.; Zhang, C.; He, H.; Teraoka, Y. Promotion effect of residual K on the decomposition of N₂O over cobalt–cerium mixed oxide catalyst. *Catal. Today* 2007, 126, 449–455.
48. Mei, Y.; Meisheng, C.; Zhang, N.; Zhiqi, L.; Huang, X. Characterization of CeO₂–ZrO₂ mixed oxides prepared by two different co-precipitation methods. *J. Rare Earths* 2013, 31, 251–256.
49. Luhui, W.; Hui, L.; Yuan, L.; Ying, C.; Shuqing, Y. Effect of precipitants on Ni-CeO₂ catalysts prepared by a co-precipitation method for the reverse water-gas shift reaction. *J. Rare Earths* 2013, 31, 969–974.
50. Dai, B.; Cao, S.; Xie, H.; Zhou, G.; Chen, S. Reduction of CO₂ to CO via reverse water-gas shift reaction over CeO₂ catalyst. *Korean J. Chem. Eng.* 2018, 35, 421–427.
51. Chen, X.; Su, X.; Liang, B.; Yang, X.; Ren, X.; Duan, H.; Huang, Y.; Zhang, T. Identification of relevant active sites and a mechanism study for reverse water gas shift reaction over Pt/CeO₂ catalysts. *J. Energy Chem.* 2016, 25, 1051–1057.
52. Ronda-Lloret, M.; Rico-Francés, S.; Sepúlveda-Escribano, A.; Ramos-Fernandez, E.V. CuOx/CeO₂ catalyst derived from metal organic framework for reverse water-gas shift reaction. *Appl. Catal. A: Gen.* 2018, 562, 28–36.
53. Kim, T.K.; Lee, K.J.; Cheon, J.Y.; Lee, J.H.; Joo, S.H.; Moon, H.R. Nanoporous metal oxides with tunable and nanocrystalline frameworks via conversion of metal–organic frameworks. *J. Am. Chem. Soc.* 2013, 135, 8940–8946.
54. Liu, L.; Fan, F.; Bai, M.; Xue, F.; Ma, X.; Jiang, Z.; Fang, T. Mechanistic study of methanol synthesis from CO₂ hydrogenation on Rh-doped Cu (111) surfaces. *Mol. Catal.* 2019, 466, 26–36.
55. Lykaki, M.; Pachatouridou, E.; Carabineiro, S.A.; Iliopoulou, E.; Andriopoulou, C.; Kallithrakas-Kontos, N.; Boghosian, S.; Konsolakis, M. Ceria nanoparticles shape effects on the structural defects and surface chemistry: Implications in CO oxidation by Cu/CeO₂ catalysts. *Appl. Catal. B: Environ.* 2018, 230, 18–28.
56. Zheng, X.; Li, Y.; Zhang, L.; Shen, L.; Xiao, Y.; Zhang, Y.; Au, C.; Jiang, L. Insight into the effect of morphology on catalytic performance of porous CeO₂ nanocrystals for H₂S selective oxidation. *Appl. Catal. B Environ.* 2019, 252, 98–110.
57. Kovacevic, M.; Mojet, B.L.; van Ommen, J.G.; Lefferts, L. Effects of morphology of cerium oxide catalysts for reverse water gas shift reaction. *Catal. Lett.* 2016, 146, 770–777.
58. Lin, L.; Yao, S.; Liu, Z.; Zhang, F.; Li, N.; Vovchok, D.; Martinez-Arias, A.; Castañeda, R.; Lin, J.; Senanayake, S.D. In situ characterization of Cu/CeO₂ nanocatalysts for CO₂ hydrogenation: Morphological effects of nanostructured ceria on the catalytic activity. *J. Phys. Chem. C* 2018, 122, 12934–12943.
59. Liu, Y.; Li, Z.; Xu, H.; Han, Y. Reverse water–gas shift reaction over ceria nanocube synthesized by hydrothermal method. *Catal. Commun.* 2016, 76, 1–6.
60. Esch, F.; Fabris, S.; Zhou, L.; Montini, T.; Africh, C.; Fornasiero, P.; Comelli, G.; Rosei, R. Electron localization determines defect formation on ceria substrates. *Science* 2005, 309, 752–755.

61. Skorodumova, N.; Baudin, M.; Hermansson, K. Surface properties of CeO₂ from first principles. *Phys. Rev. B* 2004, 69, 075401.
62. Zhang, Y.; Liang, L.; Chen, Z.; Wen, J.; Zhong, W.; Zou, S.; Fu, M.; Chen, L.; Ye, D. Highly efficient Cu/CeO₂-hollow nanospheres catalyst for the reverse water-gas shift reaction: Investigation on the role of oxygen vacancies through in situ UV-Raman and DRIFTS. *Appl. Surf. Sci.* 2020, 516, 146035.
63. Konsolakis, M.; Lykaki, M.; Stefa, S.; Carabineiro, S.A.; Varvoutis, G.; Papista, E.; Marnellos, G.E. CO₂ hydrogenation over nanoceria-supported transition metal catalysts: Role of ceria morphology (nanorods versus nanocubes) and active phase nature (Co versus Cu). *Nanomaterials* 2019, 9, 1739.
64. Kim, M.-S.; Chung, S.-H.; Yoo, C.-J.; Lee, M.S.; Cho, I.-H.; Lee, D.-W.; Lee, K.-Y. Catalytic reduction of nitrate in water over Pd–Cu/TiO₂ catalyst: Effect of the strong metal-support interaction (SMSI) on the catalytic activity. *Appl. Catal. B Environ.* 2013, 142, 354–361.
65. Liotta, L.; Longo, A.; Macaluso, A.; Martorana, A.; Pantaleo, G.; Venezia, A.; Deganello, G. Influence of the SMSI effect on the catalytic activity of a Pt (1%)/Ce_{0.6}Zr_{0.4}O₂ catalyst: SAXS, XRD, XPS and TPR investigations. *Appl. Catal. B Environ.* 2004, 48, 133–149.
66. Bertella, F.; Concepción, P.; Martínez, A. The impact of support surface area on the SMSI decoration effect and catalytic performance for Fischer-Tropsch synthesis of Co-Ru/TiO₂-anatase catalysts. *Catal. Today* 2017, 296, 170–180.
67. Tauster, S.; Fung, S.; Garten, R.L. Strong metal-support interactions. Group 8 noble metals supported on titanium dioxide. *J. Am. Chem. Soc.* 1978, 100, 170–175.
68. Hosokawa, S.; Taniguchi, M.; Utani, K.; Kanai, H.; Imamura, S. Affinity order among noble metals and CeO₂. *Appl. Catal. A: Gen.* 2005, 289, 115–120.
69. Ivanova, A.; Slavinskaya, E.; Gulyaev, R.; Zaikovskii, V.; Stonkus, O.; Danilova, I.; Plyasova, L.; Polukhina, I.; Boronin, A. Metal–support interactions in Pt/Al₂O₃ and Pd/Al₂O₃ catalysts for CO oxidation. *Appl. Catal. B Environ.* 2010, 97, 57–71.
70. Strobel, R.; Pratsinis, S.E. Flame synthesis of supported platinum group metals for catalysis and sensors. *Platin. Met. Rev.* 2009, 53, 11–20.
71. Goguet, A.; Meunier, F.C.; Tibiletti, D.; Breen, J.P.; Burch, R. Spectrokinetic investigation of reverse water-gas-shift reaction intermediates over a Pt/CeO₂ catalyst. *J. Phys. Chem. B* 2004, 108, 20240–20246.
72. Zou, H.; Dong, X.; Lin, W. Selective CO oxidation in hydrogen-rich gas over CuO/CeO₂ catalysts. *Appl. Surf. Sci.* 2006, 253, 2893–2898.
73. Zhou, G.; Xie, F.; Deng, L.; Zhang, G.; Xie, H. Supported mesoporous Cu/CeO₂- δ catalyst for CO₂ reverse water–gas shift reaction to syngas. *Int. J. Hydrogen Energy* 2020, 45, 11380–11393.
74. Aitbekova, A.; Wu, L.; Wrasman, C.J.; Boubnov, A.; Hoffman, A.S.; Goodman, E.D.; Bare, S.R.; Cargnello, M. Low-temperature restructuring of CeO₂-supported Ru nanoparticles determines selectivity in CO₂ catalytic reduction. *J. Am. Chem. Soc.* 2018, 140, 13736–13745.
75. Tauster, S. Strong metal-support interactions. *Acc. Chem. Res.* 1987, 20, 389–394.
76. Matte, L.P.; Kilian, A.S.; Luza, L.; Alves, M.C.; Morais, J.; Baptista, D.L.; Dupont, J.; Bernardi, F. Influence of the CeO₂ support on the reduction properties of Cu/CeO₂ and Ni/CeO₂ nanoparticles. *J. Phys. Chem. C* 2015, 119, 26459–26470.
77. Thill, A.S.; Kilian, A.S.; Bernardi, F. Key role played by metallic nanoparticles on the ceria reduction. *J. Phys. Chem. C* 2017, 121, 25323–25332.
78. Figueiredo, W.T.; Escudero, C.; Perez-Dieste, V.; Ospina, C.A.; Bernardi, F. Determining the Surface Atomic Population of Cu_xNi_{1-x}/CeO₂ (0 < x ≤ 1) Nanoparticles during the Reverse Water–Gas Shift (RWGS) Reaction. *J. Phys. Chem. C* 2020, 124, 16868–16878.
79. Einakchi, R. Metal Nanoparticles Over Active Ionic-Conductive Supports for the Reverse Water Gas Shift Reaction. Master's Dissertation, Université d'Ottawa/University of Ottawa, Ottawa, ON, Canada, 2016.
80. Wang, L.; Liu, H.; Chen, Y.; Yang, S. Reverse water–gas shift reaction over co-precipitated Co–CeO₂ catalysts: Effect of Co content on selectivity and carbon formation. *Int. J. Hydrogen Energy* 2017, 42, 3682–3689.
81. Wang, L.; Liu, H. Mesoporous Co–CeO₂ catalyst prepared by colloidal solution combustion method for reverse water-gas shift reaction. *Catal. Today* 2018, 316, 155–161.
82. Jurković, D.L.; Pohar, A.; Dasireddy, V.D.; Likozar, B. Effect of copper-based catalyst support on reverse water-gas shift reaction (RWGS) activity for CO₂ reduction. *Chem. Eng. Technol.* 2017, 40, 973–980.

83. Bouarab, R.; Akdim, O.; Auroux, A.; Cherifi, O.; Mirodatos, C. Effect of MgO additive on catalytic properties of Co/SiO₂ in the dry reforming of methane. *Appl. Catal. A Gen.* 2004, 264, 161–168.
84. Pino, L.; Vita, A.; Cipiti, F.; Laganà, M.; Recupero, V. Hydrogen production by methane tri-reforming process over Ni-ceria catalysts: Effect of La-doping. *Appl. Catal. B Environ.* 2011, 104, 64–73.
85. Zhu, M.; Ge, Q.; Zhu, X. Catalytic reduction of CO₂ to CO via reverse water gas shift reaction: Recent advances in the design of active and selective supported metal catalysts. *Trans. Tianjin Univ.* 2020, 26, 172–187.
86. Chen, X.; Su, X.; Duan, H.; Liang, B.; Huang, Y.; Zhang, T. Catalytic performance of the Pt/TiO₂ catalysts in reverse water gas shift reaction: Controlled product selectivity and a mechanism study. *Catal. Today* 2017, 281, 312–318.
87. Liu, L.; Corma, A. Metal catalysts for heterogeneous catalysis: From single atoms to nanoclusters and nanoparticles. *Chem. Rev.* 2018, 118, 4981–5079.
88. Li, S.; Xu, Y.; Chen, Y.; Li, W.; Lin, L.; Li, M.; Deng, Y.; Wang, X.; Ge, B.; Yang, C. Tuning the selectivity of catalytic carbon dioxide hydrogenation over iridium/cerium oxide catalysts with a strong metal–support interaction. *Angew. Chem.* 2017, 129, 10901–10905.
89. Chen, X.; Chen, Y.; Song, C.; Ji, P.; Wang, N.; Wang, W.; Cui, L. Recent advances in supported metal catalysts and oxide catalysts for the reverse water-gas shift reaction. *Front. Chem.* 2020, 8, 709.
90. Zhao, Z.; Wang, M.; Ma, P.; Zheng, Y.; Chen, J.; Li, H.; Zhang, X.; Zheng, K.; Kuang, Q.; Xie, Z.-X. Atomically dispersed Pt/CeO₂ catalyst with superior CO selectivity in reverse water gas shift reaction. *Appl. Catal. B Environ.* 2021, 291, 120101.
91. Lu, B.; Kawamoto, K. Preparation of mesoporous CeO₂ and monodispersed NiO particles in CeO₂, and enhanced selectivity of NiO/CeO₂ for reverse water gas shift reaction. *Mater. Res. Bull.* 2014, 53, 70–78.
92. Wang, W.; Zhang, Y.; Wang, Z.; Yan, J.-M.; Ge, Q.; Liu, C.-J. Reverse water gas shift over In₂O₃–CeO₂ catalysts. *Catal. Today* 2016, 259, 402–408.
93. Ro, I.; Sener, C.; Stadelman, T.M.; Ball, M.R.; Venegas, J.M.; Burt, S.P.; Hermans, I.; Dumesic, J.A.; Huber, G.W. Measurement of intrinsic catalytic activity of Pt monometallic and Pt–MoO_x interfacial sites over visible light enhanced PtMoO_x/SiO₂ catalyst in reverse water gas shift reaction. *J. Catal.* 2016, 344, 784–794.
94. Pettigrew, D.; Trimm, D.; Cant, N. The effects of rare earth oxides on the reverse water-gas shift reaction on palladium/alumina. *Catal. Lett.* 1994, 28, 313–319.
95. Yang, L.; Pastor-Pérez, L.; Gu, S.; Sepúlveda-Escribano, A.; Reina, T. Highly efficient Ni/CeO₂–Al₂O₃ catalysts for CO₂ upgrading via reverse water-gas shift: Effect of selected transition metal promoters. *Appl. Catal. B Environ.* 2018, 232, 464–471.
96. Wang, L.; Widmann, D.; Behm, R.J. Reactive removal of surface oxygen by H₂, CO and CO/H₂ on a Au/CeO₂ catalyst and its relevance to the preferential CO oxidation (PROX) and reverse water gas shift (RWGS) reaction. *Catal. Sci. Technol.* 2015, 5, 925–941.
97. Lee, S.M.; Eom, H.; Kim, S.S. A study on the effect of CeO₂ addition to a Pt/TiO₂ catalyst on the reverse water gas shift reaction. *Environ. Technol.* 2021, 42, 182–192.
98. Zhao, B.; Pan, Y.-X.; Liu, C.-J. The promotion effect of CeO₂ on CO₂ adsorption and hydrogenation over Ga₂O₃. *Catal. Today* 2012, 194, 60–64.
99. Dai, H.; Zhang, A.; Xiong, S.; Xiao, X.; Zhou, C.; Pan, Y. The Catalytic Performance of Ga₂O₃–CeO₂ Composite Oxides over Reverse Water Gas Shift Reaction. *ChemCatChem* 2022, 14, e202200049.
100. Dorner, R.W.; Hardy, D.R.; Williams, F.W.; Willauer, H.D. Effects of ceria-doping on a CO₂ hydrogenation iron–manganese catalyst. *Catal. Commun.* 2010, 11, 816–819.
101. Galvita, V.V.; Poelman, H.; Bliznuk, V.; Detavernier, C.; Marin, G.B. CeO₂-modified Fe₂O₃ for CO₂ utilization via chemical looping. *Ind. Eng. Chem. Res.* 2013, 52, 8416–8426.
102. Yan, B.; Zhao, B.; Kattel, S.; Wu, Q.; Yao, S.; Su, D.; Chen, J.G. Tuning CO₂ hydrogenation selectivity via metal-oxide interfacial sites. *J. Catal.* 2019, 374, 60–71.
103. Rahmani, F.; Haghighi, M.; Estifaei, P. Synthesis and characterization of Pt/Al₂O₃–CeO₂ nanocatalyst used for toluene abatement from waste gas streams at low temperature: Conventional vs. plasma–ultrasound hybrid synthesis methods. *Microporous Mesoporous Mater.* 2014, 185, 213–223.
104. Zonetti, P.C.; Letichevsky, S.; Gaspar, A.B.; Sousa-Aguiar, E.F.; Appel, L.G. The Ni_xCe_{1-x}O. 75Zr_{0.25}–xO₂ solid solution and the RWGS. *Appl. Catal. A Gen.* 2014, 475, 48–54.
105. Wenzel, M.; Rihko-Struckmann, L.; Sundmacher, K. Continuous production of CO from CO₂ by RWGS chemical looping in fixed and fluidized bed reactors. *Chem. Eng. J.* 2018, 336, 278–296.

106. Yang, L.; Pastor-Pérez, L.; Villora-Picó, J.J.; Gu, S.; Sepúlveda-Escribano, A.; Reina, T.R. CO₂ valorisation via reverse water-gas shift reaction using promoted Fe/CeO₂-Al₂O₃ catalysts: Showcasing the potential of advanced catalysts to explore new processes design. *Appl. Catal. A Gen.* 2020, 593, 117442.
107. Ray, K.; Sengupta, S.; Deo, G. Reforming and cracking of CH₄ over Al₂O₃ supported Ni, Ni-Fe and Ni-Co catalysts. *Fuel Proces. Technol.* 2017, 156, 195–203.
108. Theofanidis, S.A.; Galvita, V.V.; Poelman, H.; Marin, G.B. Enhanced carbon-resistant dry reforming Fe-Ni catalyst: Role of Fe. *Acs Catal.* 2015, 5, 3028–3039.
109. Chen, L.; Wu, D.; Wang, C.; Ji, M.; Wu, Z. Study on Cu-Fe/CeO₂ bimetallic catalyst for reverse water gas shift reaction. *J. Environ. Chem. Eng.* 2021, 9, 105183.
110. Li, M.; My Pham, T.H.; Ko, Y.; Zhao, K.; Zhong, L.; Luo, W.; Züttel, A. Support-Dependent Cu-In Bimetallic Catalysts for Tailoring the Activity of Reverse Water Gas Shift Reaction. *ACS Sustain. Chem. Eng.* 2022, 10, 1524–1535.

Retrieved from <https://encyclopedia.pub/entry/history/show/69022>